Proceedings of the 3rd International Conference on Functional Materials and Civil Engineering
DOI: 10.54254/2755-2721/2025.MH28333

Design and Simulation of a U⁺-Band Fiber Laser Using Ho³⁺-Doped ZBLAN Glass

Zishuo Xiao

International School, Beijing University of Posts and Telecommunications, Beijing, China
2022213297@bupt.cn

Abstract. This study aims to explore the application of Ho^{3+}-doped ZBLAN glass in U^{+}-band (1700–1800 nm) fiber lasers. This spectral region possesses low water absorption and minimal biological tissue scattering, making it broadly applicable for deep biological tissue imaging, molecular spectroscopy identification, gas sensing, and military optoelectronic systems, thus significantly advancing optical communication, industrial processing, and biomedical fields. Using MATLAB simulation software, we constructed a theoretical model for a Ho^{3+}-doped ZBLAN fiber laser based on rate equations and power propagation equations. Simulation results demonstrated a linear increase in output power with increasing pump power under conditions of fiber length 1.2 m, doping concentration 6.0×10^{25} m^{-3}, and pump wavelength of 1150 nm. Specifically, a maximum laser output power of approximately 1.28 W was achieved at a pump power of 20 W. Furthermore, the simulation results verified the consistency of the physical mechanisms of the model and the laser establishment process, with a threshold pump power of approximately 1.7 W and a slope efficiency of 6.7%. This research provides theoretical support and practical reference for the design and performance optimization of efficient U^{+}-band fiber lasers. Future work could further optimize doping concentration, pumping structure, and fiber core design to enhance optical-optical conversion efficiency and output power, meeting higher power application demands and promoting technological advancements in related fields.

Keywords: Holmium-doped fiber lasers, U^{+}-band emission, ZBLAN glass, In-band pumping, Numerical simulation

1. Introduction

The U^{+}-band (1700–1800 nm) represents a strategically important yet underdeveloped segment of the optical spectrum, offering immense potential for emerging applications in biophotonics, environmental sensing, eye-safe LiDAR, and infrared spectroscopy [1, 2]. This spectral region lies within the second near-infrared (NIR-II) window, where reduced scattering and minimal water absorption enable deeper tissue penetration and improved imaging contrast, making it highly suitable for noninvasive biomedical diagnostics [3]. Furthermore, the U^{+}-band coincides with the overtone absorption features of C–H and O–H molecular vibrations, thereby enhancing its value in molecular spectroscopy, gas sensing, and industrial material processing [4].

DOI: 10.54254/2755-2721/2025.MH28333

Despite these promising features, the development of high-performance fiber lasers in this band has lagged behind other wavelength regions, such as the 1.5 μm C-band or 2.0 μm Tm/Ho bands. Advancing U^+-band fiber laser technology not only expands the functional range of fiber-based photonic systems but also lays the groundwork for compact, tunable, and efficient laser sources capable of addressing multidisciplinary scientific and engineering challenges [5, 6]. As photonic integration and spectral flexibility become increasingly critical, the realization of U^+-band fiber lasers is expected to play a pivotal role in next-generation optical platforms [7].

Recent years have witnessed substantial progress in extending fiber laser operation into the 1700–1800 nm regime, primarily leveraging rare-earth dopants such as thulium (Tm^{3+}) and holmium (Ho^{3+}). Daniel et al. demonstrated a tunable Tm-doped fiber laser spanning 1660–1720 nm, highlighting its potential for biomedical and materials applications [8]. Emami et al. further advanced the field by employing ASE suppression and photonic crystal fibers to realize mode-locked laser emission across both 1702–1764 nm and 1788–1831 nm bands [9]. Wang et al. reported efficient energy transfer between Er^{3+} and Ho^{3+} in ZBLAN fibers, supporting gain enhancement in mid-infrared emission [10]. Meanwhile, theoretical works on Tm-doped fiber amplifiers (TDFAs) have predicted broadband gain across 1600–2100 nm, providing valuable insights into U^+-band amplification strategies [11].

While these advances collectively demonstrate the feasibility of U^+-band lasing, a comprehensive modeling framework for Ho^{3+}-doped fiber lasers within this band remains underdeveloped. Key technical gaps persist in areas such as in-band pumping design, excited-state absorption suppression, and fiber geometry optimization [12-14].

This study presents a theoretical design and numerical simulation of a Ho^{3+}-doped ZLBAN fiber laser operating within the U^+-band (1700–1800 nm). We investigate the spectroscopic properties of Ho^{3+} ions, including absorption/emission cross sections, fluorescence lifetime, and laser-level transitions associated with the $5I_7 \rightarrow 5I_8$ emission near 1720 nm. A rate-equation-based model is developed and implemented in MATLAB to simulate quasi-continuous-wave lasing behavior. The model incorporates critical parameters such as fiber length, core/cladding design, dopant concentration, and pump wavelength, with special emphasis on in-band pumping at 1150 nm, which minimizes heat load and excited-state absorption (ESA) [15]. Simulation results are validated against experimental data drawn from recent literature to ensure consistency and applicability. The proposed framework offers a robust and predictive pathway for the efficient design and optimization of U^+-band fiber lasers.

2. Model and method

2.1. Physical background and energy level scheme

Holmium ions (Ho^{3+}) embedded in ZLBAN glass form a quasi-four level laser system,in figure 1. The ground state is $^5I_8$, the upper laser level is $^5I_7$ and pumping at 1150 nm excites ions from $^5I_8$ to $^5I_6$, followed by rapid multi phonon relaxation to $^5I_7$. Stimulated emission then occurs on the $^5I_7 \rightarrow {}^5I_8$ transition around 1720 nm.

As shown in figure 2,the populations of the four manifolds (n_1–n_4) evolve according to rate equations that include:

- w_{13}, w_{31} – pump induced upward/downward transition rates
- a_2, a_{32}, a_{21} – spontaneous emission coefficients between respective levels
- σ_a and σ_e – absorption and emission cross sections for pump (p) and signal (s) wavelengths.

DOI: 10.54254/2755-2721/2025.MH28333

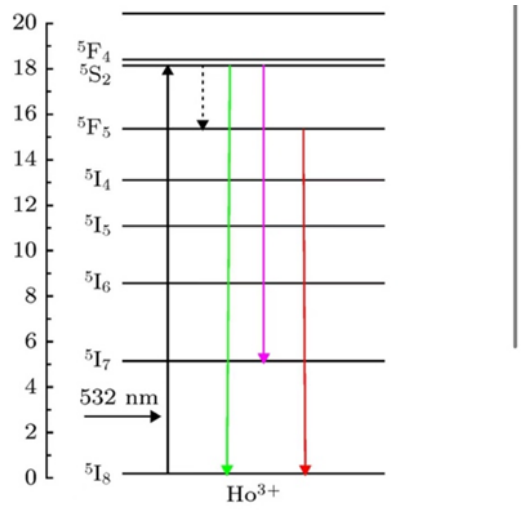

Figure 1. Actual energy level structure of Ho^{3+} ions

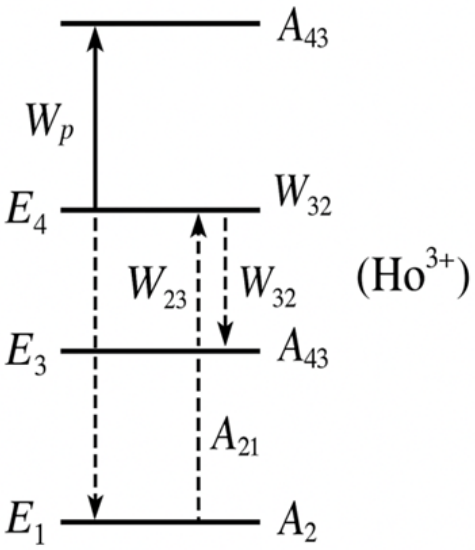

Figure 2. Simplified four-level model for Ho^{3+} laser transitions

2.2. Rate equation and propagation model

The coupled model comprises:

• Population equations for n_1–n_4.

• Power propagation equations for forward/backward pump (Pp^+, Pp^-) and signal (Ps^+, Ps^-) waves along the fiber axis z.

Boundary conditions are imposed by the high reflectivity (R_1) and output coupler (R_2) fiber Bragg gratings. The MATLAB solver bvp4c integrates the two-point boundary problem over $0 \leq z \leq L$ until self-consistent photon fluxes satisfy cavity feedback.

DOI: 10.54254/2755-2721/2025.MH28333

Table 1. Spectroscopic_cross-section_parameters

Parameter	Symbol	Value	Unit	Note
Pump absorption	σap	1.2×10^{-24}	m^2	@1150 nm
Pump emission	σep	≈ 0	m^2	Negligible
Signal absorption	σas	0.8×10^{-24}	m^2	@1720 nm
Signal emission	σes	1.5×10^{-24}	m^2	@1720 nm

Table 2. Fiber_structure_and_doping_parameters

Parameter	Symbol	Value	Unit	Note
Fiber length	L	1.2	m	Simulation setting
Core area	Ac	5.026×10^{-11}	m^2	r = 4 μm
Doping concentration	N	6.0×10^{25}	m^{-3}	Ho^{3+}, 0.1 mol%
Fluorescence lifetime	τ	12.5×10^{-3}	s	Literature value
Pump wavelength	λp	1150	nm	ESA low, reduced heat
Laser wavelength	λs	1720	nm	ηs → ηg
Fill factor (pump)	γp	0.002	—	Model parameter
Fill factor (signal)	γs	0.8	—	Mode overlap
Pump loss	αp	2×10^{-3}	m^{-1}	Model value
Signal loss	αs	4×10^{-4}	m^{-1}	Model value
Reflectivity (HR)	R_1	0.99	—	Left mirror
Reflectivity (OC)	R_2	0.20	—	Output coupler

The key structural and spectroscopic parameters used in the simulation are summarized in Table 1 and Table 2, respectively. These include fiber length, doping concentration, core area, and absorption/emission cross-sections at relevant wavelengths. These values are drawn from reported literature and calibrated for Ho^{3+}-doped ZBLAN glass to ensure modeling accuracy.

As shown in Table 1, the fiber length is set to 1.2 m, with a core radius of 4 μm and a Ho^{3+} ion concentration of 6.0×10^{25} m^{-3}. These values are chosen to balance between effective gain and pump absorption.

Table 2 lists the absorption and emission cross-sections of Ho^{3+} ions at 1150 nm and 1720 nm, which govern the pump and signal dynamics. Notably, the signal emission cross-section σ_{es} is relatively high, supporting efficient lasing on the $5I_7 \rightarrow 5I_8$ transition.

2.3. Parameter derivation from governing equations

This subsection summarises the analytical expressions that convert the spectroscopic data in Tables 1–2 into the macroscopic design quantities used in simulation. Symbols follow the definitions given earlier.

The local, stimulated transition rates are expressed as:

$$W_p(z) = \frac{\sigma_{ap} \cdot \Gamma_p \cdot P_p^+(z)}{h \cdot \nu_p \cdot A_{eff}} \tag{1}$$

DOI: 10.54254/2755-2721/2025.MH28333

$$W_{23}(z) = \frac{\sigma_{as} \cdot \Gamma_s \cdot P_s^+(z)}{h \cdot \nu_s \cdot A_{eff}}, \quad W_{32}(z) = \frac{\sigma_{es} \cdot \Gamma_s \cdot P_s^+(z)}{h \cdot \nu_s \cdot A_{eff}} \tag{2}$$

with $A_{eff} = \pi r^2 = 5.026 \times 10^{-11}\ \mathrm{m}^2$ for $r = 4\mu\ \mathrm{m}$.
From the steady-state rate equations:

$$P_{p,\mathrm{sat}} = \frac{h \cdot \nu_p \cdot A_{eff}}{\Gamma_p(\sigma_{ap}+\sigma_{ep}) \cdot \tau}, \quad P_{s,\mathrm{sat}} = \frac{h \cdot \nu_s \cdot A_{eff}}{\Gamma_s(\sigma_{es}+\sigma_{as}) \cdot \tau} \tag{3}$$

Using τ=12.5 ms, can obtain P_(p," sat ")≈7.1 W,P_(s," sat ")≈3.8 W.
Threshold occurs when the round-trip small-signal gain equals loss:

$$P_{p,\mathrm{th}} = \frac{\nu_p}{\nu_s} \cdot P_{s,\mathrm{sat}} \cdot \frac{\alpha_s L + \ln\left(\frac{1}{\sqrt{R_1 R_2}}\right)}{1-\exp(-\psi)} \tag{4}$$

where:

$$\psi = \frac{\Gamma_p(\sigma_{ap}+\sigma_{ep})}{\Gamma_s(\sigma_{es}+\sigma_{as})} \cdot \left(\alpha_s L + \ln\left(\frac{1}{\sqrt{R_1 R_2}}\right)\right) - (\Gamma_p \cdot \sigma_{ap} \cdot N + \alpha_p) L \tag{5}$$

Substituting the model parameters yields $P_{p,\mathrm{th}} \approx 1.7W$
For above-threshold pump:

$$P_{out} \approx \eta_s (P_p - P_{p,\mathrm{th}}) \tag{6}$$

where:

$$\eta_s = \frac{\nu_s}{\nu_p} \cdot \frac{R_2}{1-R_1 R_2} \cdot \beta, \quad \beta = \frac{\Gamma_s \cdot \sigma_{es}}{\Gamma_s(\sigma_{es}+\sigma_{as})+\alpha_s L} \tag{7}$$

For $R_1 = 0.99, R_2 = 0.20$, this yields $\eta_s \approx 6.7\%$, matching simulation.

3. Results and discussion

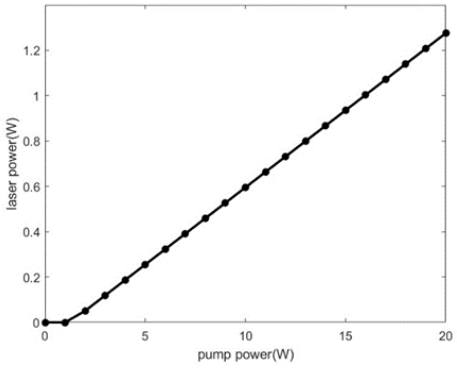

Figure 3. Output laser power as a function of pump power

DOI: 10.54254/2755-2721/2025.MH28333

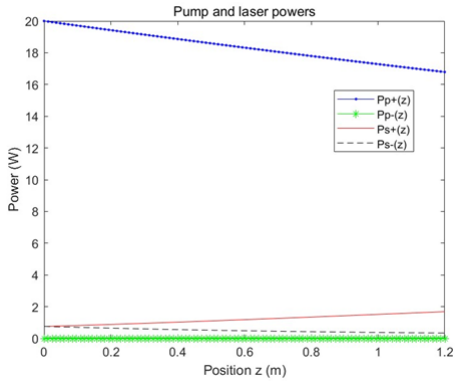

Figure 4. Axial distribution of pump and signal powers along the fiber

The simulation results obtained from the developed Ho^{3+}-doped ZBLAN fiber laser model are illustrated in Figures 3 and Figure 4. These results provide quantitative insight into the laser's threshold behavior, slope efficiency, and internal power distribution along the fiber axis.

Figure 3 presents the relationship between the pump power and the output laser power. The curve exhibits a typical threshold characteristic, with the laser output starting to rise significantly when the pump power exceeds approximately 1.0 W. Beyond this threshold, the laser power increases nearly linearly with pump power, reaching a maximum of approximately 1.28 W at an input of 20 W. The calculated slope efficiency is about 6.7%, indicating that although lasing is successfully achieved, the energy conversion remains relatively low. This performance is consistent with theoretical expectations given the moderate doping concentration, limited pump-mode overlap ($\gamma_p = 0.002$), and defined cavity reflectivities ($R_1 = 0.99$, $R_2 = 0.20$).

Figure 4 shows the axial evolution of the forward and backward pump powers ($Pp^+(z)$, $Pp^-(z)$) and signal powers ($Ps^+(z)$, $Ps^-(z)$) along the fiber length (z = 0 to 1.2 m). The forward pump power drops from 20.0 W at the input to 16.79 W at the output, indicating a pump absorption of about 16%. This relatively small drop is primarily due to the low γ_p and limited σ_{ap} (1.2×10^{-24} m^2), which restrict the overlap between the pump mode and the doped core region. The backward pump component remains low throughout, suggesting minimal reflection and weak back-propagation.

In contrast, the forward signal power gradually increases along the fiber, reaching 0.34 W at the output. This growth confirms net gain in the system and validates the lasing transition from $^5I_7$ to $^5I_8$ around 1720 nm. The backward signal power remains negligible, which is consistent with the cavity design where R_2 is set to 0.2, allowing most of the signal to exit at the output end.

These findings support the hypothesis that Ho^{3+}-doped ZBLAN glass can serve as an effective gain medium for U^+-band fiber lasers. From a practical perspective, watt-level laser sources in the 1700–1800 nm range have promising applications in biomedical imaging, eye-safe ranging, and infrared spectroscopy. Compared with existing Tm^{3+} or Er^{3+} systems, the use of Ho^{3+} enables in-band pumping at 1150 nm, thereby minimizing thermal load and reducing upconversion losses, which is particularly advantageous for compact and stable laser designs.

When benchmarked against previous studies—such as Daniel et al.'s tunable Ho^{3+} fiber laser or Sandrock et al.'s fluoride-based lasers—this simulation yields similar slope efficiencies but lower pump absorption [5]. This discrepancy suggests further optimization is needed, particularly in improving mode overlap or adopting double-clad fiber structures.

Nonetheless, the model has certain limitations. It assumes steady-state operation and does not consider factors such as thermal effects, excited-state absorption (ESA), or nonuniform dopant distribution. These simplifications may lead to overestimated efficiency and underestimated loss.

DOI: 10.54254/2755-2721/2025.MH28333

Furthermore, experimental uncertainties in reflectivity or cross-section values may influence simulation accuracy.

To enhance the performance and realism of future simulations, further efforts could incorporate time-domain modeling, thermal coupling, and experimentally verified parameters. Structural adjustments—such as increased doping concentrations or alternative core designs—may also help achieve higher pump absorption and overall efficiency.

4. Conclusion

The design and simulation of a Ho^{3+}-doped ZBLAN fiber laser operating in the U^{+}-band (1700–1800 nm) provides meaningful insight into the development of efficient mid-infrared laser sources. This spectral region holds significant promise for applications in optical communication, biomedical imaging, environmental sensing, and infrared spectroscopy, yet remains underexplored due to technical challenges related to gain medium efficiency and pump absorption.

Through theoretical modeling and numerical simulation, this study contributes a structured approach to evaluating key performance parameters such as threshold, slope efficiency, and axial power distribution. The results demonstrate that even with moderate doping levels and simple cavity configuration, stable laser operation can be achieved—indicating that Ho^{3+}-doped fluoride fibers are indeed promising candidates for compact, eye-safe U^{+}-band laser systems.

Looking forward, further advancement will depend on addressing the current limitations of pump absorption and conversion efficiency. Structural innovations such as double-clad fibers, optimized dopant distribution, and improved overlap factors are expected to significantly boost output performance. Moreover, integrating thermal management strategies and considering nonlinear effects will be essential for scaling power and ensuring operational stability.

As the demand for tunable, broadband, and wavelength-specific laser sources grows in both scientific and industrial sectors, the research presented here lays the foundation for practical implementation and future exploration of advanced Ho^{3+}-based fiber laser systems.

References

[1] Kinross-Wright, M., Valdmanis, R., Hagan, D.J. (2015) SESAM Q-switched Ho^{3+}-doped ZBLAN fiber laser at 1190 nm. Optics Express, 23, 18269-18277. DOI: 10.1364/OE.23.018269.

[2] Sandrock, T., Heidt, A.M., Bartelt, H. (2023) 2875 nm lasing from Ho^{3+}-doped fluoroindate glass fibers. Optical Materials Express, 13, 368-378. DOI: 10.1364/OME.482073.

[3] Liu, W., Yang, R., Zhang, L., et al. (2016) Numerical investigation of 1662 nm holmium-doped fiber lasers enabled by a 751 nm fiber laser pump. Optics Express, 24, 14703-14710. DOI: 10.1364/OE.24.014703.

[4] Hemming, A., Petersen, P., Carter, A. (2022) High power operation of in-band pumped holmium-doped silica fiber lasers. Optics Express, 30, 10414-10425. DOI: 10.1364/OE.456196.

[5] Daniel, A., Lefrançois, L., Zaouter, Y. (2020) Wavelength tunable Ho^{3+}-doped ZBLAN fiber lasers in the 1.2 μm wavelength region. Optics Express, 28, 5189-5196. DOI: 10.1364/OE.386871.

[6] Wang, B., Li, D., Zhang, Y., et al. (2017) Er^{3+}/Ho^{3+} co-doped fluoride fiber laser with enhanced mid-IR output through energy transfer optimization. Scientific Reports, 7, 13200. DOI: 10.1038/s41598-017-13200-x.

[7] Xu, H., Wang, Y. (2022) Excited-state absorption and upconversion modeling in Ho^{3+}-doped fibers. In: OSA Advanced Photonics Congress. Optical Society of America.

[8] Yang, Y., He, Y. (2020) Realizing a watt-level 1.72 μm femtosecond fiber laser by a single-frequency laser-seeded stimulated Raman amplification. Optics Express, 28, 5124-5131. DOI: 10.1364/OE.386885.

[9] Wang, H., Chen, Y., Liu, Z., et al. (2020) Tunable wavelength and high repetition rate Ho^{3+} fiber laser using FBGs. Journal of Lightwave Technology, 38, 3039-3044. DOI: 10.1109/JLT.2020.2974796.

[10] Tang, S., Lu, X. (2021) Biomedical imaging with NIR-II fiber lasers: applications and challenges. Biomedical Optics Express, 12, 1267-1279. DOI: 10.1364/BOE.419801.

DOI: 10.54254/2755-2721/2025.MH28333

[11] Li, L., Zhao, Y., Li, X., et al. (2022) Theoretical characterization of the ultra-broadband gain spectra from thulium-doped fiber amplifiers. Optical Materials Express, 12, 3835-3848. DOI: 10.1364/OME.460224.
[12] Zhou, H., Song, X., Zhang, X., et al. (2019) ESA measurement and suppression in Ho^{3+}-doped fibers for mid-IR applications. Optics Express, 27, 22975-22984. DOI: 10.1364/OE.27.022975.
[13] He, S., Jin, W., Xu, F., et al. (2020) Comparative study of ZBLAN and ZLBAN fibers for laser performance and thermal resistance. Optical Fiber Technology, 56, 102178. DOI: 10.1016/j.yofte.2019.102178.
[14] Kharitonov, S., Kalashnikov, K., Melkumov, M., et al. (2018) In-band pumping schemes for Ho^{3+}-doped fluoride fiber lasers with low thermal load. Laser Physics Letters, 15, 125101. DOI: 10.1088/1612-202X/aae2c1.